Intermetallics 48 (2014) 44–53

Contents lists available at ScienceDirect

Intermetallics

journal homepage: www.elsevier.com/locate/intermet

Alloying effects in polycrystalline γ′ strengthened Co–Al–W base alloys

H.-Y. Yan, V.A. Vorontsov, D. Dye*

Department of Materials, Royal School of Mines, Imperial College London, Prince Consort Road, London SW7 2BP, UK

ARTICLE INFO

Article history:
Received 25 July 2013
Received in revised form
20 October 2013
Accepted 23 October 2013
Available online 20 November 2013

Keywords:
B. Phase diagrams
B. Precipitates
B. Oxidation
A. Aluminides, miscellaneous

ABSTRACT

A polycrystalline hot working ingot metallurgy processing route for γ/γ′ Co–Al–W superalloys has been developed. Based on Co–7Al–7W (at%), substitutions of Mo, V, Ti, Ta, Ni, Si, Fe and Cr were examined. The γ′ solvus was found to follow the same trends as those exhibited by alloys with higher γ′ fractions considered by other investigators. Excessive Cr additions were found to lead to discontinuous coarsening and eventually, the loss of the γ′ phase from the microstructures observed. Ni additions were examined, with some success, and found to restore the γ′ phase and raise the solvus temperature. It was found that the addition of 13 at.% Cr improved the oxidation resistance at 800 °C by over 40 times.

1. Introduction

In 2006, Sato et al. [1] discovered a new phase in the Co–Al–W system, Co_3 (Al,W). This new $L1_2$ γ′ phase can coexist with a face centred cubic (FCC) A1 γ matrix. The lattice mismatch between the γ and γ′ phases is ~0.53% [1], allowing the precipitate-matrix interface to be coherent. Thus, the microstructure of Co–Al–W ternary alloys is similar to the Ni-base superalloys. This exciting discovery provides a possible research direction for the development of new high temperature superalloys. With incremental improvements in the temperature capability of conventional Ni-base superalloys reaching a plateau [2], this is attractive as jet engine operating efficiency improvements are driven by increases in the temperature capability of the superalloys used in hot section components such as turbine blades and discs.

The original Sato paper has now been cited over 100 times, with many groups exploring the phase metallurgy of this alloy system, although work is still at the very early stages. The γ′ fraction and solvus temperature increases with increased Al and W content [3,4]. Ti, Ta, Nb, Mo and V preferentially partition to the γ′ phase and increase the γ′ solvus temperature, whereas Cr, Mn, Fe and Re partition to the γ phase and lower the solvus temperature [3–9]. The flow stress anomaly has also been observed, with Ta additions being found to improve the alloy strength at elevated temperatures [10,11].

Shinagawa et al. [12,13] found that there is a continuous phase field linking γ′ Co_3 (Al,W) to γ′ Ni_3Al. Furthermore, there is a continuous phase field between the FCC Ni and Co phases above 422 °C [14]. At room temperature, the FCC phase can be stabilised with as little as 35 at.% Ni. This leads to the hypothesis that γ/γ′ alloys might be found anywhere along the continuum in between, and therefore the Co–Ni–Al–W system is of great interest. In particular, it was found that the solvus temperature increases with increasing Ni content and that the size of the γ + γ′ two phase field also increased with Ni content.

As well as strength, high temperature oxidation resistance is another property required of superalloys. Oxidation of the Co–Al–W γ/γ′ alloys at 800 °C results in the formation of a multi-layered oxide structure [15–19]. The outer layer has been identified as Co_3O_4, the middle layer is composed of mixed oxides of Al, W and other alloying elements, whilst the inner layer is suggested to be a continuous layer of Al_2O_3. The base metal below the growing oxide is depleted in Al and therefore the γ′ fraction decreases and elongated Co_3W precipitates are formed. The effects of alloying elements on oxidation behaviour have also been investigated in Refs. [6,15,16,18,20]. The addition of Ti, Mo and Nb to the base alloy results in decreased oxidation resistance. In contrast, Cr and Si help form highly protective oxides and therefore are beneficial for oxidation resistance.

* Corresponding author. Tel.: +44 207 594 6811.
E-mail address: david.dye@imperial.ac.uk (D. Dye).

0966-9795
http://dx.doi.org/10.1016/j.intermet.2013.10.022

In the present study, we investigate the influence of different alloying elements in Co–Al–W base alloys and their effects on the phase metallurgy and oxidation behaviour at high temperature. In particular, Cr additions are explored up to the levels used in Ni superalloys and alloys along the Co–Ni superalloy continuum are examined.

2. Experimental procedures

20 alloys were investigated in this study, Table 1. The first 10 alloys examined alloy substitutions (Mo, V, Ti, Si, Ta etc) to a Co–7Al–7W (at.%) base alloy (all compositions in this study are provided as atomic fractions). The second group of 10 alloys was divided into three subcategories. The first 4 alloys examined the effect of Cr additions on the oxidation behaviour. The Co–Al–W alloy has an FCC structure in the γ matrix and $L1_2$ structure in the γ' phase. Cr has a body centred cubic (BCC) structure. Therefore, an excessive amount of Cr added to the Co–Al–W base alloy can destabilise the γ/γ' microstructure. However, substitution of Co for Ni has been found to stabilise the γ' phase [21], so in the next 3 alloys Ni additions were made to a Co–Al–W–Cr base alloy. The final three alloys maintain the total Al and W content at 14 at.%. As Ni additions are made, the Al fraction is increased in proportion to the distance along the Co–Ni continuum [12], such that $Al/(Al + W) = 0.5 + 0.5 \times Ni/(Co + Ni)$. This also has the beneficial side effect of reducing the alloy density and, by increasing the size of the γ' phase field, improving the stability of the alloys produced.

The nominal compositions of the alloys and their respective ageing conditions are given in Table 1. 50 g finger-shaped polycrystalline ingots were produced by vacuum arc melting under a back-filled argon atmosphere. Co–10W (at.%) and Co–20W (at.%) master alloys were used along with high-purity elemental pellets of 99.99% Cr; 99.97% Ni; 99.9% Al, Ti, Ta and Si; 99.8% Co; 99.5% Mo; 99.7% V and 99.0% Fe. The as-cast ingots were then vacuum solution heat-treated at 1300 °C for 24 h. Subsequently, the ingots were encapsulated in rectilinear mild steel cans with Ti powder packing material and super solvus hot rolled at 1150 °C to a sample thickness of ~3 mm for the first 10 alloys. Similar procedures were carried out for the next 10 alloys, but to a thickness of ~6 mm. A NETZSCH Jupiter differential scanning calorimeter (DSC) was then employed to determine the solvus temperature at a 10 °C/min scan rate under an argon atmosphere. The alloys were aged at 80–100 °C below the solvus temperature. For all the ageing heat treatments, the alloys were sealed in quartz tubes which were backfilled with argon after evacuation. On completion of the heat treatment, the alloys were allowed to cool in the furnace.

Table 1
Nominal compositions of the alloys studied and ageing conditions employed.

Composition (at.%)	Abbreviation	Ageing
Co–7Al–7W	Base	765 °C/200 h
Co–7Al–5W–2Mo	2Mo	715 °C/200 h
Co–7Al–5W–2V	2V	736 °C/200 h
Co–6Al–6W–2Ti	2Ti	790 °C/200 h
Co–7Al–5W–2Ta	2Ta	900 °C/100 h
Co–7Al–7W–20Ni	20Ni	790 °C/200 h
Co–7Al–3W–6Ni–4V	6Ni–4V	741 °C/200 h
Co–7Al–7W–1Si	1Si	794 °C/200 h
Co–7Al–7W–20Fe	20Fe	689 °C/200 h
Co–7Al–7W–10Cr	10Cr	772 °C/200 h
Co–7Al–7W–13Cr	13Cr	746 °C 200/h
Co–7Al–7W–17Cr	17Cr	689 °C 200/h
Co–7Al–7W–21Cr	21Cr	637 °C 200/h
Co–7Al–7W–23Cr	23Cr	–
Co–7Al–7W–21Cr–11Ni	21Cr–11Ni	688 °C 200/h
Co–7Al–7W–21Cr–21Ni	21Cr–21Ni	726 °C 200/h
Co–7Al–7W–21Cr–32Ni	21Cr–32Ni	791 °C 200/h
Co–8Al–6W–21Cr–11Ni	21Cr–11Ni–A	689 °C 200/h
Co–9Al–5W–21Cr–21Ni	21Cr–21Ni–A	748 °C 200/h
Co–10.5Al–3.5W–21Cr–32Ni	21Cr–32Ni–A	817 °C 200/h

Table 2
Actual compositions, solvus temperatures, densities (ρ) and Vickers hardness (HV) of the alloys. Starred solvus temperatures indicate alloys where a γ' volume fraction could not be determined (Fig. 2).

Alloy	Composition at.%			Solvus	ρ	HV
	Al	W	Other	°C	g cm^{-3}	
Base	7.3	6.8		854	9.18	468
2Mo	7.2	4.7	1.8Mo	804	8.92	406
2V	7.3	4.8	2.1V	825	8.50	404
2Ti	6.4	6.0	2.2Ti	919	9.16	410
2Ta	9.9	4.8	1.8Ta	983	9.09	434
20Ni	7.3	7.0	20.2Ni	881	9.29	348
6Ni–4V	7.7	3.0	6.4Ni–4.2V	830	8.58	323
1Si	7.2	7.2	0.7Si	883	9.25	427
20Fe	7.3	7.0	19.5Fe	778*	9.04	568
10Cr	7.2	6.8	9.8Cr	861	9.29	347
13Cr	7.4	7.1	13.2Cr	835	9.39	395
17Cr	7.5	7.0	17.3Cr	778*	9.13	640
21Cr	7.6	7.2	21.3Cr	726*	9.16	681
23Cr	4.8	6.6	22.9Cr	–*	8.78	326
21Cr–11Ni	7.5	7.2	20.8Cr–11.1Ni	777*	9.13	463
21Cr–21Ni	6.9	7.3	21.5Cr–21.7Ni	815	9.07	461
21Cr–32Ni	7.7	6.5	20.8Cr–33.2Ni	880	9.09	383
21Cr–11Ni–A	8.5	5.5	21.0Cr–10.9Ni	778*	8.89	323
21Cr–21Ni–A	9.3	4.7	21.1Cr–21.3Ni	837	8.69	401
21Cr–32Ni–A	11.2	3.4	20.5Cr–32.5Ni	906	8.36	388

Alloy compositions were measured using Inductively Coupled Plasma-Optical Emission Spectroscopy (ICP-OES) at Incotest, Hereford, UK. Both density measurements and Vickers hardness tests were performed according to ASTM B311-08 and ASTM E92-82 at room temperature.

The microstructure of the alloy was examined using the LEO1525 field emission gun scanning electron microscope (FEG-SEM) in the secondary electron imaging mode. Secondary phase compositions were measured using energy dispersive X-ray spectroscopy (EDS) The samples were ground, polished and electro-etched in a solution of 2.5% phosphoric acid in methanol at 2.5 V at room temperature for a few seconds.

Cyclic oxidation experiments were performed using $2.5 \times 2.5 \times 2.5$ mm cubes, mechanically ground to a surface finish of 0.25 μm, cleaned and degreased. Flat-bottomed alumina crucibles were used to contain the samples which were oxidation tested in air at 800 °C. To contain any spallation products, lids were placed on the crucibles during the periodic specimen removal and air cooling prior to the weighing of the crucibles and specimens. The mass change was measured after 4, 16, 36, 64, 100, 144 and 196 h of oxidation.

3. Results and discussion

The actual compositions, γ' solvus temperatures, densities and the Vickers hardness values of all the alloys are listed in Table 2, in the fully aged condition. It should be noted that the Al content was slightly higher than the nominal composition in all the alloys, because an extra 0.5 wt.% of Al was added to each alloy to compensate for the evaporation of Al during melting. The desired compositions for all the alloys were achieved within 1.2 at.%, with the exception of the Al content in the 23Cr alloy.

Visible light and secondary electron micrographs for the base ternary alloy, Co–7Al–7W, are shown in Fig. 1. The grain size was approximately 50 μm. Because of the growth and recovery mechanisms occurring during long ageing heat treatment, annealing twins are typically observed inside the grains [22]. The

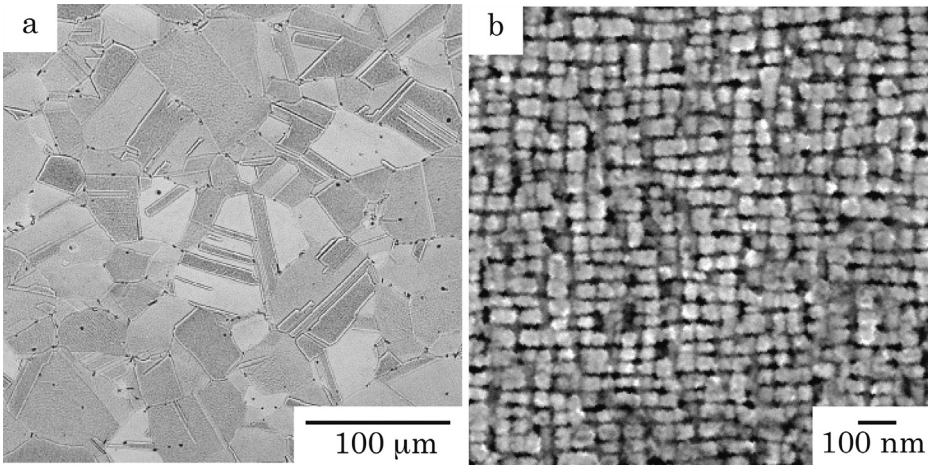

Fig. 1. (a) Light micrograph of the hot rolled base alloy; (b) Secondary electron image of the heat treated base alloy.

microstructure in the secondary electron image was obtained after sub-solvus ageing for 200 h. Cuboidal γ' precipitates were observed in a γ matrix. Despite the long ageing heat treatment of 200 h, the γ' precipitates were very small, on the order of 20 nm.

Returning to Table 2, Co–7Al–7W has a density of 9.18 g cm^{-3} which is higher than most Ni-base superalloys [23]. To achieve lower density in this alloy system, the refractory metal (W) content needs to be reduced. Therefore, the goal is to reduce the W content by alloying lighter elements into the base alloy whilst still achieving a γ/γ' microstructure with a sufficiently high solvus temperature.

The 2Mo, 2V and 6Ni–4V alloys show that reducing the W content reduces the alloy density while still retaining the desired microstructure. Alloying 1 at.% of Si into the base alloy is not sufficient to reduce the alloy density; any effect is overwhelmed by the experimental variation in W content. 2Ti substitution for 1Al–1W had minimal effect on density. The substitution of W for Ta, as well as Co for Fe, Cr and Ni, also had minimal effects on the density, as might be expected given their atomic masses. The final three alloys, denoted by –A, also show the effect of W content; the density reduces monotonically as W is replaced by Al, towards that of a modern low refractory Ni-base superalloy.

The area fraction of the γ' phase was obtained from thresholding SEM images in the ImageJ software package to produce a binary γ and γ' image. Three SEM images were analysed from different grains such that the area fraction is representative of the alloy and so it can be assumed that the area fraction of the γ' phase is the γ' volume fraction. However, this approach only measures the secondary γ' fraction, and ignores the fine (<10 nm) tertiary γ'.

Fig. 2 summarises the effect of composition on the γ' solvus temperature and also considers the attainable γ' volume fraction, in the context of the literature. The first observation is that the solvus temperature and volume fraction increase as W is added, making the alloys super-stoichiometric. However, it has now been shown [9] that the Al solubility in the matrix is higher than that of W, so alloys with more W than Al will find it easier to form stoichiometric Co_3 (Al,W) and hence W additions have a disproportionate effect.

Additions of Ti, Ta and Ni increase the solvus, especially Ta, which can increase the solvus temperature by more than 100 °C. Cr appears to increase the γ' fraction but not solvus temperature. Mo appears to decease the solvus; substitutions for W increase the fraction slightly whilst additions decrease it. In both Co–7Al–7W and Co–9Al–10W, Si additions decrease the fraction markedly, but the effect on the solvus is less clear. 20 at.% Fe in the Co–7Al–7W base decreases the solvus temperature and this agrees with Ooshima et al. [3].

Mo additions to Co–9Al–7W and Co–9Al–10W decrease the γ' fraction, whereas in the present study Mo substitution for W in Co–7Al–7W increased it. Noticeably, Ni additions decreased the fraction very significantly. It may be that some fine tertiary γ' were also present, as can be observed in the 2Ti and 2Ta alloys, but the fractions of fine tertiary γ' could not be reliably assessed using secondary electron imaging of the etched samples, and so are not included in the fractions assessed here.

In Co–9Al–7W, V increased the solvus and γ' fraction, whereas in Co–9Al–10W, V decreased both solvus and fraction. Here, in Co–7Al–7W, V substitution for W increased the fraction enormously at the cost of a decreased solvus. However, in the presence of Ni the fraction and solvus remained the same. Hence, it appears that V is a γ' former, at least in the case of alloys such as the ones considered here that are, due to the higher solubility for Al than W in the matrix, relatively lean in W content. However, for alloys that are W-rich, the V is neutral or partitions to the matrix.

There are some caveats to be made when making comparisons between different groups' findings in Fig. 2. Ooshima et al. [3] aged their Co–9Al–7W based alloys at 850 °C for 96 h, at temperatures 100–220 °C below the solvus, and tertiary γ' were not observed. Similarly, Xue et al.'s [8] Co–9Al–10W based alloys were aged at

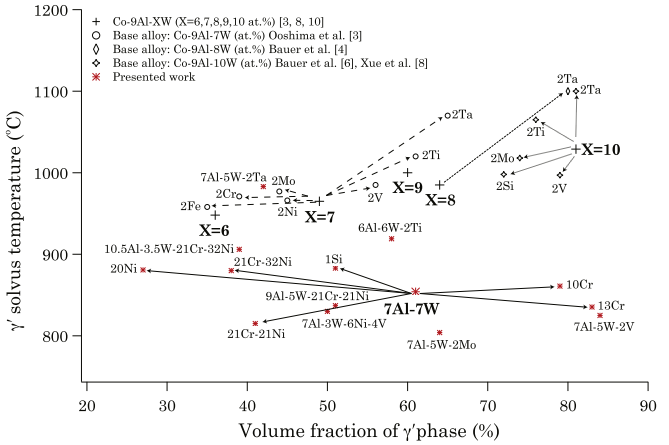

Fig. 2. Effect of alloying additions and substitutions on the γ' solvus temperature and volume fraction of secondary γ', compared to the literature.

900 °C, 100–200 °C below the solvus for 300 h, and no tertiary γ' were observed. Here, we aged 80–100 °C below the solvus, and quite frequently tertiary γ' appeared, which are not included in the fractions measured in Fig. 2. Thus, our volume fractions represent a minimum estimate. However, the discussion above is felt to be robust to these comments.

Small additions of Cr to Co–7Al–7W increase the solvus temperature and the volume fraction of γ' phase, as shown in Fig. 2. Cr additions are desirable, as chromia is usually protective and therefore it is likely that Cr will improve oxidation resistance. However, beyond 10Cr the solvus decreases and the desirable γ' morphology can no longer be achieved. Instead of forming as fine precipitates, the γ' is observed as elongated lamellae. It appears that excessive Cr additions destabilise the γ/γ' microstructure, until in the Co–7Al–7W–23Cr alloy no solvus could be found. Addition of 21 at.% of Cr to the base alloy lowered the solvus temperature by 128 °C.

Shinagawa et al. [12] found that Ni increases the solvus and widens the $\gamma + \gamma'$ phase field. Our results for alloys based on Co–7Al–7W–21Cr, Table 2, show that Ni additions can restore the cuboidal γ' microstructure when in sufficient quantity. This is very significant as it suggests that it may be possible to produce Co–Ni superalloys with sufficient tolerance for Cr to be oxidation resistant. The final three alloys that follow this idea, compensating for increasing Ni content by increasing the Al/W ratio, show a similar effect, but with slightly elevated volume fractions and solvus temperatures compared to their-7Al–7W counterparts. Of course, these changes also decrease density very significantly.

3.1. Secondary phases

Sato et al. [1] claimed that in the Co–Al–W ternary system the γ' phase is stable at 900 °C, but is metastable at 1000 °C. They observed the γ' phase to co-exist with the A1 γ-Co, B2 β-CoAl, DO_{19} χ-Co_3W and D_{85} μ-Co_7W_6 phases at 900 °C. More recently, Kobayashi et al. [24] showed that γ' is metastable at 900 °C, decomposing into γ, CoAl and Co_3W after 2000 h. Therefore a consensus seems to be emerging that in the Co–Al–W ternary the γ' is metastable. Alloying refractory metals into the system has been observed to promote the formation of both Co_3W and Co_7W_6 [8]. These secondary phases in the system may be detrimental to the mechanical properties of the alloy and so it is important to understand the effect of other additions on the phase equilibria.

Backscattered electron images at low magnifications for all the alloys showing secondary intermetallic phases are shown in Fig. 3, *i.e.* all except 2V, 20Ni, 6Ni–4V. Also, the 23Cr alloy is excluded. Quite commonly in these 16 alloys, secondary phases are observed after heat treatment, and these have been identified using point EDS. Table 3 lists the compositions of the secondary phases observed Fig. 3.

The dark contrast phase in the 1Si alloy is β, a B2-ordered intermetallic, formed during cooling from solution heat treatment at 1300 °C. This phase has previously been observed [8,24]. The compositions of B2 observed fall into two groups; those in the simple ternary, 2Mo and 1Si alloys that have nearly 50% Al, and

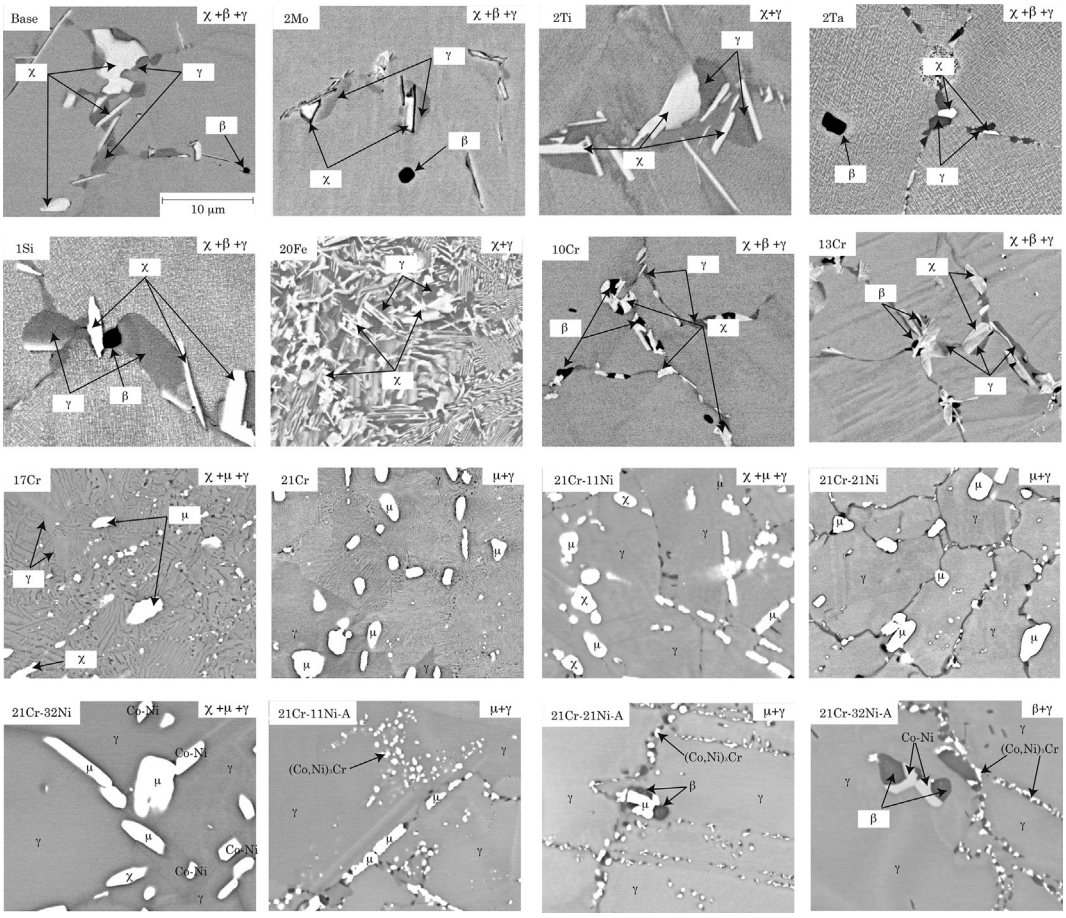

Fig. 3. Low magnification BSEI micrographs for the 16 alloys (lightly etched) showing undesirable secondary phases, after ageing heat treatment. The secondary phases have been identified, as indicated, by point EDS.

Table 3
Compositions of the secondary phases, in at.%, found in the alloys examined after ageing heat treatment, measured by EDS and averaged over at least 5 different points in each case (to 2s.f.).

Alloy	γ (A1)						β (B2)						χ (DO_{19})						μ (D_{85})				
	Co	Ni	Cr	Al	W		Co	Ni	Cr	Al	W		Co	Ni	Cr	Al	W		Co	Ni	Cr	Al	W
Base	91			6.6	2.7		56			41	3.0		78			4.5	17				–		
2Mo	92			4.8	1.7	1.5Mo	43			54	1.7	1.4Mo	77			4.1	13	6.1Mo			–		
2V				–						–						–					–		
2Ti	89			6.7	3.5	1.2Ti				–			77			3.8	15	4.1Ti			–		
2Ta	82			10	5.6	2.2Ta	67			28	2.7	1.8Ta	76			5.2	12	6.9Ta			–		
20Ni				–						–						–					–		
6Ni–4V				–						–						–					–		
1Si	88			8.1	4.4		47			51	2.2		75			3.9	21				–		
20Fe	61			11	3.3	25Fe				–			68			3.5	19	10Fe			–		
10Cr	76		12	5.9	5.6		64		7.4	23	6.2		72		9.7	3.7	14				–		
13Cr	73		14	5.4	7.2		62		9.4	24	4.4		72		13	3.1	12				–		
17Cr	69		18	7.5	5.8					–			61		17	5.2	17		49		14		37
21Cr	69		21	6.9	5.0					–						–			45		18	5.1	32
21Cr–11Ni	55	12	22	7.3	4.8					–			48	8.6	21	3.7	20		40	4.6	18		37
21Cr–21Ni	45	21	21	6.9	5.7					–						–			36	8.4	19		37
21Cr–32Ni	32	33	21	7.8	5.3					–			31	25	22	4.5	18		29	13	19		39
21Cr–11Ni–A	53	11	22	7.8	5.8					–						–			42	7.0	20		31
21Cr–21Ni–A	44	21	21	8.8	5.7		24	33	7.2	33	3.4					–			35	12	19	6.7	27
21Cr–32Ni–A	33	32	22	10	4.1		15	43	6.1	35	0.6					–					–		

those associated with Ta and Cr additions that have lower Al contents. Quite often, where B2 phase has formed then adjacent to it a region of Co-rich (A1) phase is found that is free of γ'.

The χ DO_{19} phase is also frequently observed, appearing as bright (high-Z) phases in the micrographs. Taking the Base, 2Ta and 1Si micrographs as exemplars, it appears that the A1 phase has decomposed into a 3-phase mixture of A1, χ and β, particularly in the region of grain boundaries. Away from these regions, the desired A1-γ/γ' microstructure is observed (albeit directionally coarsened in the 20Fe, 17Cr and 21Cr alloys). The formation of the

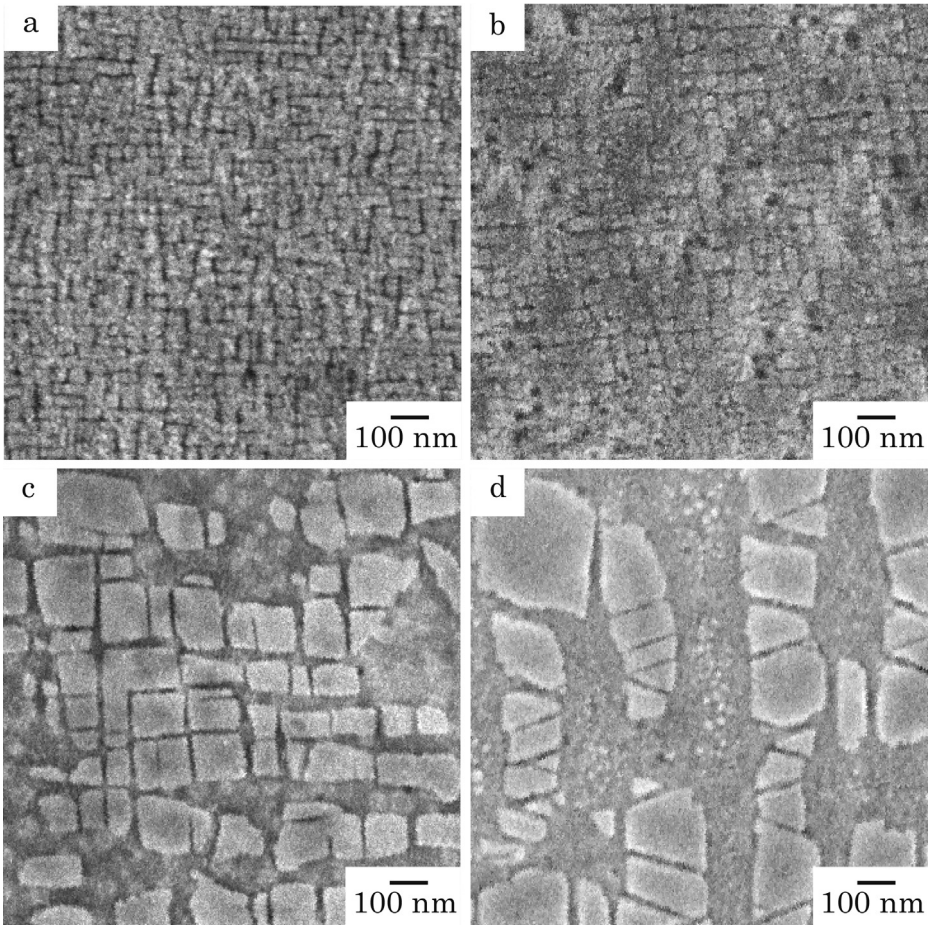

Fig. 4. Secondary electron images of heat treated Co–Al–W base alloys with addition of (a) 2Mo, (b) 2V, (c) 2Ti and (d) 2Ta.

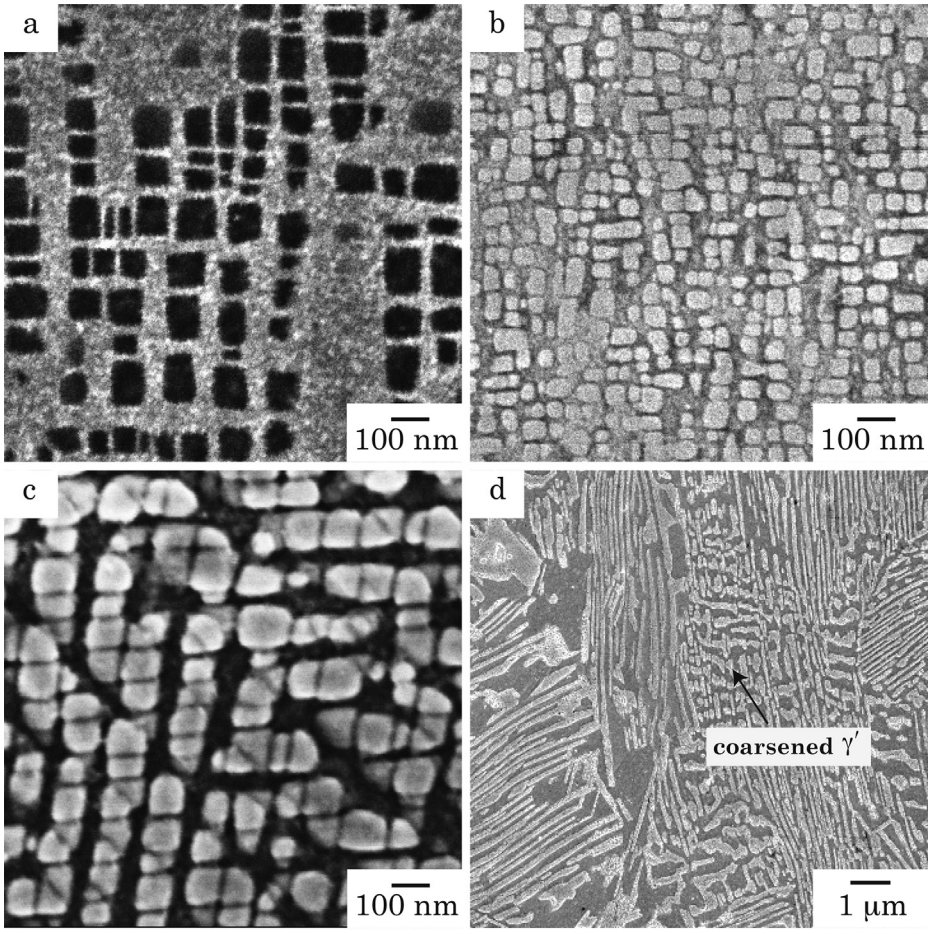

Fig. 5. Secondary electron images of heat treated Co–Al–W base alloys with addition of (a) 20Ni, (b) 6Ni–4V, (c) 1Si and (d) 20Fe.

Co_3W phase is by a peritectoid reaction between the γ-Co and the Co_7W_6 phase upon cooling [25,26].

In contrast, the major secondary phase in the alloys with >17 at.% Cr is μ Co_7W_6. It primarily formed during solution heat treatment at 1300 °C. In addition, some traces of Co_3W can be found in the alloys. Due to heavy elements in both types of precipitate, they both appear in bright contrast in the image, but can readily be distinguished in EDS from their W contents.

The small circular <1 μm precipitates in the –A alloys where the Ni addition has been balanced by changing the Al/W ratio are rather small for analysis by EDS in the SEM with its sampling volume of characteristic length ~6 μm. However, based on the literature, morphology and EDS observation of elevated W contents, they are tentatively assigned as $(Co,Ni)_3Cr$.

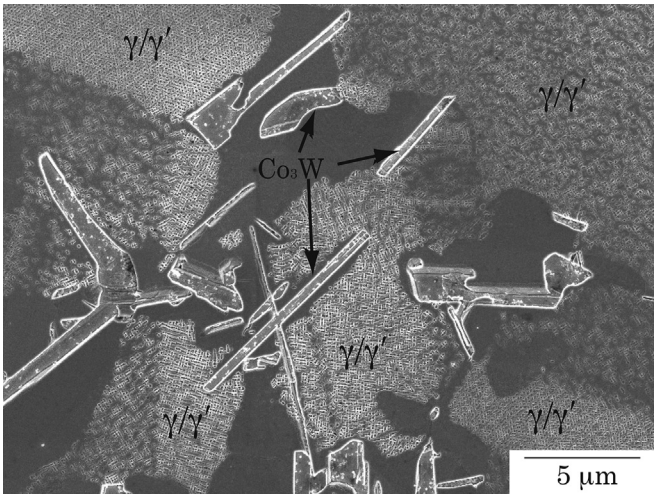

Fig. 6. 1Si alloy observed at low magnification using secondary electron imaging. Pockets of γ/γ′ are observed, as well as pockets of γ phase only. The effect is most noticeable when etched using the Spar etchant [18], as has been done here.

3.2. γ′ distribution

Fig. 4a and b shows that both Co–7Al–5W–2Mo and Co–7Al–5W–2V produce very fine cuboidal γ′ precipitates (~20 nm in size) after 200 h ageing heat treatment. Xue et al. [8] examined the addition of 2 at.% Mo and 2 at.% V into Co–9Al–10W, and heat treated for 50 h and 300 h at a much higher temperature. Consequently, the γ′ they observed were much coarser.

As for Ni base superalloys, Ti and Ta in Co–Al–W are strong γ′ stabilizing elements [13]. Therefore, we were able to age at higher temperatures and consequently observe a larger γ′ size in the 2Ti and 2Ta alloys than in the base alloy. The γ′ precipitates in the 2Ti alloy are on average ~100 nm in size. The 2Ta alloy had an average secondary γ′ size of ~150 nm. Precipitates lose coherency as the lattice misfit increases. Furthermore, large lattice misfit contributes to the driving force for coarsening via coalescence of precipitates. Both are detrimental to the creep strength [27]. Tertiary γ′ precipitates were also observed in both of these alloys, consistent with precipitation of fine cooling γ′.

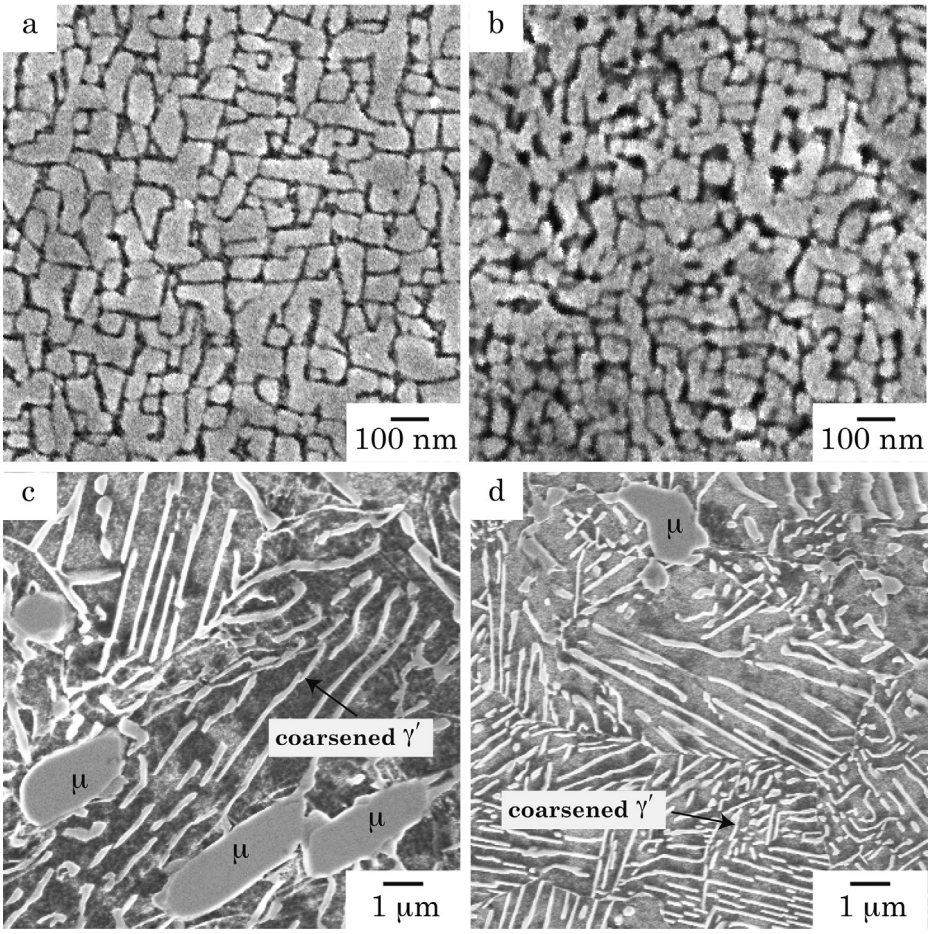

Fig. 7. Secondary electron images of Cr containing alloys (a) 10Cr, (b)13Cr, (c) 17Cr and (d) 21Cr.

The lattice misfit values for these two alloys have been recently determined using the X-ray synchrotron by Yan et al. [18], and are around +0.5%, compared to around −0.2% in Ni-base superalloys [28]. The lattice misfit in the 2Ta alloy is higher than that in the 2Ti alloy. This offers a possible explanation for the observation that the 2Ta alloy coarsened more rapidly than the 2Ti alloy. Although, given the differences in solvus, ageing temperatures and ageing time, this comparison should be treated with caution. Despite the fact that the Ta containing alloy had a greater coarsening rate, a recent report [6] shows that alloying Ta into the Co–Al–W base alloy effectively improves the creep strength. The coarsening rate for these Co–Al–W base alloys still remains unquantified. Further investigations are needed to understand (i) the diffusivity and solubility of secondary additions (and even W) in the Co matrix, (ii) the interfacial energy between the γ and γ′ phases, (iii) how the lattice misfit changes with temperature.

Fig. 5 shows that the average size of the γ′ in the 20Ni alloy was ~80 nm, whereas in the 6Ni–4V alloy, the average precipitate size was ~50 nm. However, the solvus, ageing temperature and volume fraction are different. With the 20Ni alloy being aged at a higher temperature, which would increase the coarsening rate. In the 20Ni alloy the etchant used became a γ′ etch instead of the γ etch found in the base ternary Co–Al–W system. Hence, the γ′ appear to change from white to black in secondary electron imaging. This effect can also be observed in Shinagawa et al. [12].

The addition of 1 at.% Si to the Co–Al–W system did not produce a continuous γ/γ′ microstructure, Fig. 6 Pockets of the desirable γ/γ′ microstructure exist, with average precipitate size ~100 nm, Fig. 5(c). The alloy with 20 at.% Fe did not produce the desired γ/γ′ microstructure. Instead, discontinuous coarsening was observed, see Fig. 5(d). Recently, Bauer et al. [6] examined the effect of alloying Fe into the Co–9Al–9W–0.12B base alloy. A stable γ/γ′ microstructure was observed in the Co–9Al–9W–8Fe–0.12B alloy, but as the Fe content increases to 16 at.%, the γ/γ′ microstructure ceased to exist. Both experiments show that too much Fe content in the Co–Al–W system destabilises the γ/γ′ microstructure.

Fig. 7 shows that as the Cr content was increased, the γ/γ′ microstructure became less stable. With addition of 10 at.% Cr to the base alloy, the γ′ became more rounded with an average γ′ size of ~80 nm. After a further increase in the Cr content to 13 at.%, the γ/γ′ microstructure was still observed, Fig. 7(b). Further increasing the Cr content to 17 at.% and 21 at.% resulted in discontinuous precipitation and an absence of cuboidal γ′. This is in agreement with Bauer et al. [6]. The blocky precipitates are the μ and χ phases discussed previously.

Co–7Al–7W–21Cr–11Ni (Fig. 8(a)) did not produce a γ/γ′ microstructure, neither did Co–8Al–6W–21Cr–11Ni. Both these alloys contained a large amount of μ Co_7W_6 precipitates, with small amounts of γ′ around them. Fine γ′ precipitates were observed in Co–7Al–7W–21Cr–21Ni, demonstrating that increasing the Ni content acts to stabilise the γ′, widening the phase field as suggested by Shinagawa et al. [12] In the Co–9Al–5W–21Cr–21Ni alloy, the average size of the precipitates was much larger than in the Co–7Al–7W–21Cr–21Ni alloy. Similarly, in the Co–10.5Al–3.5W–21Cr–32Ni alloy, the average precipitate size was also larger than in Co–7Al–7W–21Cr–32Ni. Therefore, replacing W with Al

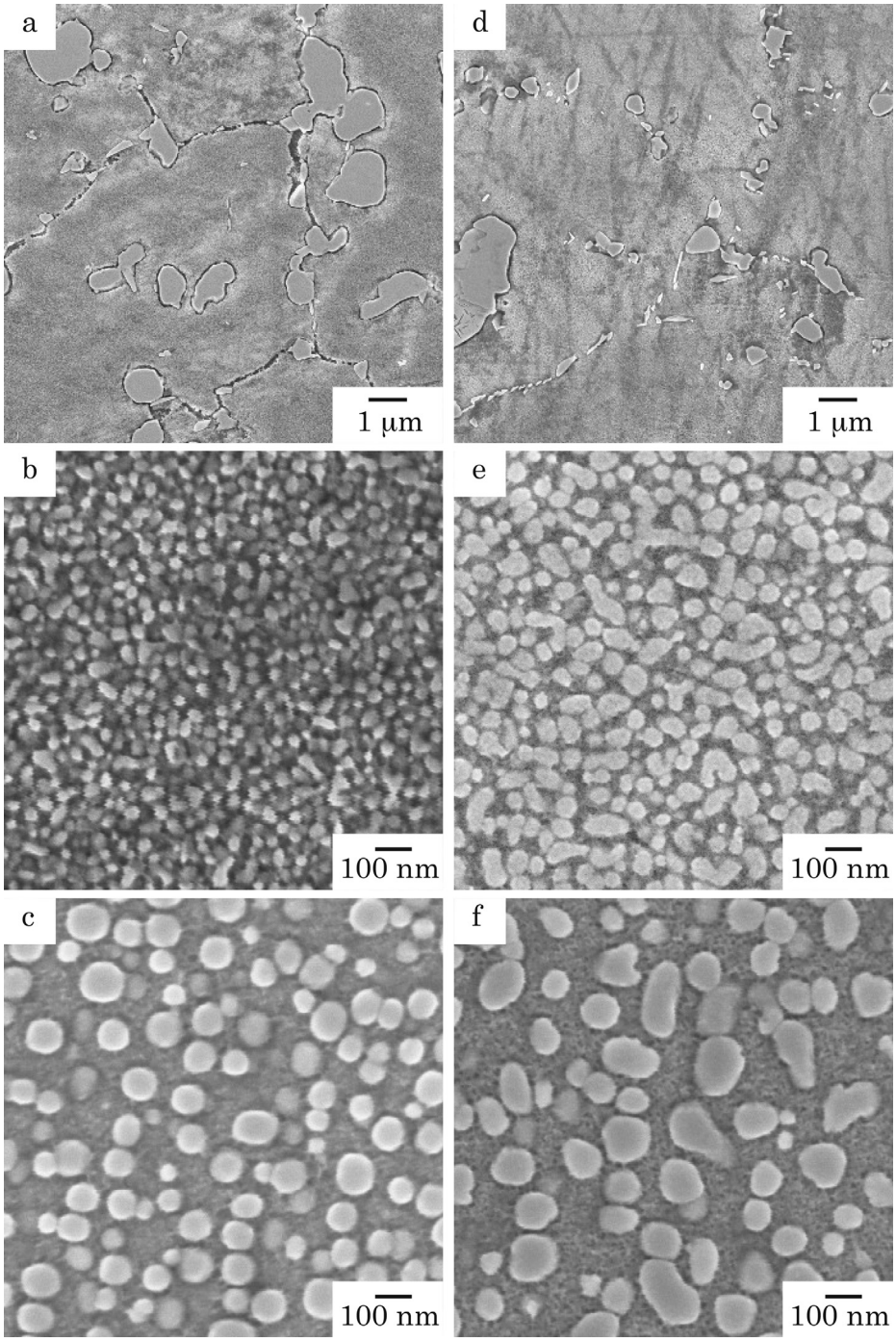

Fig. 8. Secondary electron images of (a) 21Cr–11Ni, (b) 21Cr–21Ni, (c) 21Cr–32Ni, (d) 21Cr–11Ni–A, (e) 21Cr–21Ni–A and (f) 21Cr–32Ni–A.

appears to increase the coarsening rate, as might be expected given the higher solubility of Al in the A1 matrix phase (p.109 of Ref. [28]). The shape of the γ' also becomes more spherical as the Ni content is increased, as observed by Shinagawa et al. [12] It is widely accepted that the γ' morphology changes from cuboidal to spherical due to a decrease in lattice misfit.

3.3. Cyclic oxidation

The effect of the basic quaternary alloying elements on the oxidation behaviour was examined using a cyclic oxidation experiment in air at 800 °C for 196 h, Fig. 9.

It should be noted that spallation occurred on all of the first 10 alloys during cooling. Therefore, it is difficult to determine the oxidation kinetics of the alloys. The efficacy of the different additions at limiting oxidation, in decreasing order, are found to be Cr, Fe, Si, Ta, Ni, Ti, Mo, V at 800 °C. Our results agreed with Xu et al. [21] that the effect the alloying elements on the oxidation resistance is in the order Ta > Ti > Mo at 800 °C. Furthermore, the results also agree with Klein et al. [16,17], that adding Si and Cr to the alloy improved oxidation resistance.

Fig. 9 also shows that adding V to the alloy (2V alloy) reduced the oxidation resistance quite dramatically. Moreover, comparing the 20Ni alloy to the base alloy, alloying with Ni does not improve

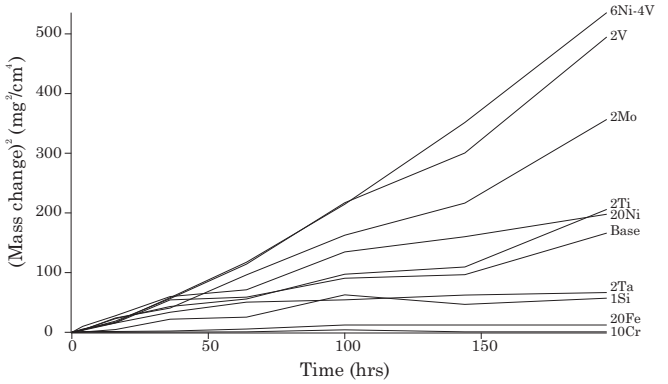

Fig. 9. Mass change data for the first 10 quaternary Co–Al–W base alloys from the cyclic oxidation experiment plotted as (mass change)^2 against time.

the oxidation resistance. Therefore, 6Ni–4V alloy is the weakest performing alloy in terms of oxidation behaviour. The 20Fe alloy has a better oxidation resistance than 1Si alloy, but alloying with Si and Cr results in formation of protective oxide scales. Unlike Si and Cr, addition of Fe does not provide a protective oxide.

The oxide scales were very similar in morphology and phases observed. An example of secondary electron image of the base alloy after 196 h exposure in air at 800 °C shown in Fig. 10. Three layers of oxides can be observed, which can be distinguished on the basis of composition. Area EDS (20 μm × 20 μm) in the JEOL JSM 6400 scanning electron microscope was used to arrive at this determination. In the base alloy, the outer layer had a measured composition of 61 Co–39 O (at.%), which has been previously referred to as either CoO [29] or Co_3O_4 [19]. The inner layer has both an outer part with composition 32 Co–9Al–10W–49O, and an inner part with similar O content but contains less Al, implying that there is outward migration of Al to the top of the inner layer. Klein et al. [17] claim that the outer part of the inner layer contains some Al_2O_3, consistent with this finding. In the base metal below, there is a corresponding Al-depleted zone containing $\gamma + \chi$ Co_3W. Between the two oxide layers and the base metal Kirkendall voids can be observed, which will tend to weaken the adherence of the oxide layers and promote spallation.

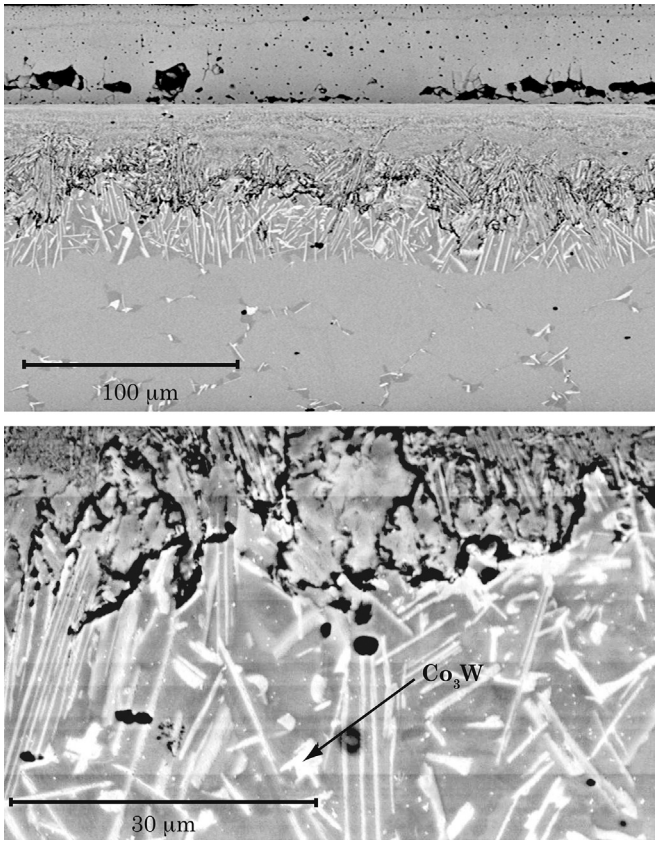

Fig. 10. Secondary electron image of the base alloy after 196 h exposure in air at 800 °C. Micrograph from sample thermally cycled without the use of a lid to contain spallation products.

Table 4 provides the mass change data for the Cr and Ni–Cr alloys. It is observed that the mass of the 10Cr and 13Cr alloys decreased after 144 h exposure time. This was due to spallation that was not contained by adding lids during cooling. Moreover, negative mass change data was recorded in the 13Cr alloy after 36 h exposure time. No spallation was observed in the 17Cr, 21Cr and 23Cr alloys, whilst the mass of these alloys is very stable, indicating that these alloys had good oxidation resistance. Unfortunately, the amount of Cr in these alloys was so great that it destabilised the γ/γ' microstructure.

The 21Cr–11Ni alloy showed poor oxidation resistance, presumably because it lacked a γ/γ' microstructure. In contrast, the 21Ni, 32Ni, and final alloys with additional Al all showed stable oxide film growth. However, it should be noted that none approached the efficacy of the 13Cr addition to the base alloy, that very high Ni additions were slightly detrimental, and that Al additions resulted in smaller mass gains.

These results indicate that improved oxidation resistance can be obtained in Co-base superalloys: in the 800 °C, 196 h condition, a mass gain in the 13Cr alloy of 0.3 mg cm^{-2} is over 40X better than in the base Co–7Al–7W alloy (mass gain of 12.9 mg cm^{-2}).

4. Conclusions

- A polycrystalline hot working ingot metallurgy processing route has been demonstrated and applied to a series of Co–Al–W base alloys.
- The expected trends in γ' content, solvus temperature and density are reproduced.

Mo, V, Fe lower the solvus temperature. Due to their lower atomic mass, V and Fe additions reduce density.

Ti and Ta raise the solvus temperature, with the substitution of −2Ta for W increasing the solvus by over 150 °C. This alloy coarsened quite rapidly on ageing, and appeared to possess a further population of tertiary γ'.

Cr additions lower the solvus temperature, and too much Cr can destabilise the γ/γ' microstructure.

Ni additions increased the solvus, but reduced the observable γ' fraction. In the −21Cr containing alloys, Ni additions stabilised the γ/γ' phase assemblage, presumably by extending the size of the γ' phase field.

- Hardness testing showed that alloys suffering discontinuous precipitation had higher hardness. Secondary phases also resulted in very high hardness.
- Undesirable secondary phases are often found in the Co superalloys, with the γ' phase co-existing with the Co-γ matrix, CoAl, Co_3W and Co_7W_6. Most of the secondary phases are present after solution heat treatment.
- Cuboid shaped γ' precipitates are observed in most of the quaternary alloys; spherical shaped γ' precipitates are produced when the Ni content is increased.

Table 4
Mass change data (mg cm^{-2}) for different at.% Cr or Ni content in the second series of Co–Al–W base alloys subjected to cyclic oxidation.

Al–W content	7Al–7W	7Al–7W	7Al–7W	7Al–7W	7Al–7W	7Al–7W	7Al–7W	7Al–7W	8Al–6W	9Al–5W	10.5Al–3.5W
Time (hrs)	10Cr	13Cr	17Cr	21Cr	23Cr	21Cr–11Ni	21Cr–21Ni	21Cr–32Ni	21Cr–11Ni	21Cr–21Ni	21Cr–32Ni
0	0	0	0	0	0	0	0	0	0	0	0
4	0	0	0	0	0	0	0	0	0	0	0
16	0	0	0.5	0.2	0.7	0.2	0.3	0.5	0.5	0	1.4
36	0.6	−0.3	1.0	0.2	0.7	1.9	0.3	1.3	1.0	0.5	1.6
64	0.9	−0.3	1.0	0.7	0.7	2.1	1.4	1.3	1.4	0.5	1.6
100	2.0	1.2	1.0	0.7	0.7	3.0	0.8	1.3	1.0	0.5	1.4
144	0.9	0.3	1.0	0.7	0.7	3.7	0.8	1.3	1.0	0.5	1.4
196	0.9	0.3	1.0	0.7	0.7	4.0	0.8	1.3	1.0	0.5	1.4

- The cyclic oxidation results show the oxide scales exhibit a three-layered structure. The cobalt oxide scales formed are not protective and suffered from spallation on cooling during cyclic oxidation testing. The base metal below the oxide scale depleted of Al, forming a region of γ matrix and elongated Co_3W precipitates. At 800 °C in air, alloying V, Mo, Ti, Ni into the alloys reduced the oxidation resistance, whereas Ta, Si, Fe and Cr addition were beneficial for the oxidation behaviour.

Acknowledgements

The authors would like to acknowledge the financial support provided by Rolls-Royce plc. and EPSRC (UK) under the Dorothy Hodgkin Postgraduate Awards scheme (H-Y.Y) and by grant EP/H004882/1 (D.D., V.A.V.). Useful conversations with Mark Hardy at Rolls-Royce plc. are also acknowledged. We would also like to thank Richard Sweeney, Mahmoud Ardakani, Matthias Knop and Nicholas G Jones for their assistance, as well as Kevin Roberts at the University of Cambridge.

References

[1] Sato J, Omori T, Oikawa K, Ohnuma I, Kainuma R, Ishida K. Cobalt-base high-temperature alloys. Science 2006;312:90–1.
[2] Reed RC. The superalloys fundamentals and applications. 1st ed. Cambridge University Press; 2006.
[3] Ooshima M, Tanaka K, Okamoto NL, Kishida K, Inui H. Effects of quaternary alloying elements on the γ′ solvus temperature of Co–Al–W based alloys with fcc/L12 two-phase microstructures. J Alloy Compd 2010;508:71–8.
[4] Bauer A, Neumeier S, Pyczak F, Göken M. Microstructure and creep strength of different γ/γ′-strengthened Co-base superalloy variants. Scr Mater 2010;63:1197–200.
[5] Cui C, Ping D, Gu Y, Harada H. A new Co-base superalloy strengthened by γ′ phase. Mater Trans 2006;47:2099–102.
[6] Bauer A, Neumeier S, Pyczak F, Göken M. Creep strength and microstructure of polycrystalline γ′-strengthened cobalt-base superalloys. In: Superalloys 2012: 12th international symposium on superalloys 2012. p. 695–703.
[7] Omori T, Oikawa K, Sato J, Ohnuma I, Kattner UR, Kainuma R, et al. Partition behavior of alloying elements and phase transformation temperatures in Co–Al–W-base quaternary systems. Intermetallics 2013:274–83.
[8] Xue F, Wang M, Feng Q. Alloying effects on heat-treated microstructure in Co–Al–W–base superalloys at 1300 °C and 900 °C. In: Superalloys 2012: 12th international symposium on superalloys 2012. p. 813–21.
[9] Meher S, Yan H-Y, Nag S, Dye D, Banerjee R. Solute partitioning and site preference in γ/γ′ cobalt-base alloys. Scr Mater 2012;67:850–3.
[10] Suzuki A, DeNolf GC, Pollock TM. Flow stress anomalies in γ/γ′ two-phase Co–Al–W-base alloys. Scr Mater 2007;56:385–8.
[11] Suzuki A, Pollock TM. High-temperature strength and deformation of γ/γ′ two-phase Co–Al–W-base alloys. Acta Mater 2008;56:1288–97.
[12] Shinagawa K, Omori T, Sato J, Oikawa K, Ohnuma I, Kainuma R, et al. Phase equilibria and microstructure on γ′ phase in Co–Ni–Al–W system. Mater Trans 2008;49:1474–9.
[13] Ishida K. Intermetallic compounds in Co-base alloys phase stability and application to superalloys. MRS Proc 2009;1128:U06–06.
[14] Nishizawa T, Ishida K. Co (cobalt) binary phase diagrams, ASM phase diagrams. ASM International; 19922.140–52.
[15] Xu Y-T, Xia T-D, Yan J-Q, Zhao W-J. Effect of alloying elements on oxidation behavior of Co–Al–W alloys at high temperature. Chin J Nonferrous Met 2010;20:2168–77.
[16] Klein L, Shen Y, Killian MS, Virtanen S. Effect of B and Cr on the high temperature oxidation behaviour of novel γ/γ′-stregthened Co-base superalloys. Corrosion Sci 2011;53:2713–20.
[17] Klein L, Bauer A, Neumeier S, Göken M, Virtanen S. High temperature oxidation of γ/γ′ strengthened Co-base superalloys. Corrosion Sci 2011;53:2027–34.
[18] Yan H-Y, Vorontsov VA, Coakley J, Jones NG, Stone HJ, Dye D. Quaternary alloying effects and the prospects for a new generation of Co-base superalloys. In: Superalloys 2012: 12th international symposium on superalloys 2012. p. 705–14.
[19] Klein L, Virtanen S. Corrosion properties of novel γ′-strengthened Co-base superalloys. Corrosion Sci 2013;66:233–41.
[20] Klein L, Virtanen S. Electrochemical characterisation of novel γ/γ′-strengthened Co-base superalloys. Electrochim Acta 2012;76:275–81.
[21] Kainuma R, Ise M, Jia C-C, Ohtani H, Ishida K. Phase equilibria and microstructural control in the Ni–Co–Al system. Intermetallics 1996;4:S151–8.
[22] Mahajan S. Critique of mechanisms of formation of deformation, annealing and growth twins: face-centered cubic metals and alloys. Scr Mater 2013;68:95–9.
[23] Davis J, editor. Nickel, cobalt and their alloys. ASM International; 2000.
[24] Kobayashi S, Tsukamoto Y, Takasugi T, Chinen H, Omori T, Ishida K, et al. Determination of phase equilibria in the Co-rich Co–Al–W ternary system with a diffusion-couple technique. Intermetallics 2009;17:1085–9.
[25] Naidu SN, Sriramamurthy A, Rao PR. The Co–W (cobalt–tungsten) system. J Alloy Phase Diag 1986;2:43–52.
[26] Miura S, Ohkubo K, Mohri T. Mechanical properties of Co-based $L1_2$ intermetallic compound Co_3 (Al,W). Mater Trans 2007;48:2403–8.
[27] Cahn R, Haasen P, editors. Physical metallurgy, vol. 1. Elsevier Science B.V.; 1996.
[28] Sims C, Stoloff N, Hagel W. Superalloys II: high temperature materials for aerospace and industrial power. John Wiley and Sons; 1987.
[29] Pollock T, Dibbern J, Tsunekane M, Zhu J, Suzuki A. New Co-based γ–γ′ high-temperature alloys. JOM 2010;62:58–63.